A SECOND ORDER CONSERVATIVE TIME-STAGGERED SCHEME FOR ALL SPEED FLOW

Amino, H.[1,2], Flageul, C.[3], Benhamadouche, S.[1,2], Tiselj, I.[4], Carissimo, B.[1,2], Ferrand, M.[1,2]

[1]EDF R&D, Fluid Mechanics, Energy and Environment Dept., Chatou, France
[2]CEREA, Ecole des Ponts, EDF R&D, Chatou, France
[3]PPRIME Institute, Curiosity Group, Université de Poitiers, CNRS, ISAE-ENSMA, France
[4]Reactor engineering division, Jožef Stefan Institute, Ljubljana, Slovenia

ABSTRACT

A time-staggered scheme for variable density flow is presented. The compressible Navier–Stokes equations are used by this pressure correction scheme which is implemented in the collocated finite-volumes open-source computational fluid dynamics solver code_saturne. The Helmholtz equation is solved for the pressure increment, taking the thermodynamic pressure into account and avoiding the acoustic time step limitation. The internal energy equation is used to compute the temperature and a numerical analysis providing conditions ensuring the positivity of the thermodynamic variables is proposed. The scheme accuracy is first verified on a 0-D pressure cooker system. Then, a discontinuous shock problem shows its capability to reproduce shocks correctly and finally, the scheme is validated on a natural convection numerical reference case.

1 WORK OVERVIEW

Designing time schemes for Computational Fluid Dynamics (CFD) that are able to cover both compressible and incompressible regimes is a challenging [1] research topic which has been given attention in the last decades [2][3][4][5][6]. Based on Pierce and Moin [7] finite difference time staggered scheme, we present a finite volumes conservative second-order time scheme for variable density flow. The proposed semi implicit pressure correction [8] scheme uses the compressible Navier–Stokes equations and is designed for regular and discontinuous solutions. The latter is implemented in the open-source CFD solver code_saturne [9] and validated against analytical and reference test cases.

Inner iterations are performed for each time step, characterised by the upper-script k and the scheme variable arrangement depends on the parameter θ ($\theta = 1$ for Implicit Euler or $1/2$ for Crank Nicolson): for instance, the momentum equation is solved between times $n-1+\theta$ and $n+\theta, k$:

$$\frac{\Theta\left(\rho^{n},\rho^{n+1,k-1}\right)\underline{\widetilde{u}}^{k}-\Theta\left(\rho^{n-1},\rho^{n,k-1}\right)\underline{u}^{n-1+\theta}}{\Delta t}+\mathrm{div}\left(\Theta\left(\underline{u}^{n-1+\theta},\underline{\widetilde{u}}^{k}\right)\otimes\underline{q}\big|_{n-1+\theta}^{n+\theta,k-1}\right)=\underline{\nabla}\,p\big|_{n-1+\theta}^{n+\theta,k-1}+\mathrm{div}\left(\underline{\underline{\tau}}^{k}\right), \tag{1}$$

where ρ is the density, $\underline{u}$ the velocity, $\underline{q}=\rho\underline{u}$ the momentum and $p|_{n-1+\theta}^{n+\theta}$ the mechanical pressure. $\Theta(\cdot)$ is the temporal interpolation of a given field. If $\theta = 1/2$ the velocity location is at the centre of the time interval $[n, n+1]$ whereas other fields are evaluated respectively on times n and $n+1$ (Fig.1). The internal energy equation is used to compute the temperature as in [10]:

$$\begin{aligned}c_v\left[\frac{\rho^{n+1,k-1}T^{n+1,k}-\rho^{n,k-1}T^{n}}{\Delta t}+\mathrm{div}\left(\Theta\left(T^{n},T^{n+1,k}\right)\underline{q}\big|_{n}^{n+1,k-1}\right)\right]&=\underline{\underline{\tau}}^{n+\theta,k-1}:\underline{\nabla u}^{n+\theta,k-1}+\Gamma^{u^2/2}\Big|_{n}^{n+1,k-1}\\ +\underline{\nabla}\cdot\left(\lambda\underline{\nabla}\Theta\left(T^{n},T^{n+1,k}\right)\right)-\mathrm{div}\left(\Theta\left(p^{n},p^{n+1,k-1}\right)\underline{u}^{n+\theta,k-1}\right)&+\underline{u}^{n+\theta,k-1}\cdot\underline{\nabla}\,p\big|_{n-1+\theta}^{n+\theta,k-1}\end{aligned} \tag{2}$$

T is the temperature, c_v the heat capacity and λ the thermal conductivity. Following [10], $\Gamma^{u^2/2}$ is a corrective source term derived from the discrete kinetic energy equation; for refined grids, the total energy

*Corresponding author: martin.ferrand@edf.fr

is conserved. The time scheme includes the effect of the thermodynamic pressure in the correction step by solving the following Helmholtz equation for $p^{n+1,k}$:

$$\begin{aligned}
&\frac{\rho^{n+1,k}-\rho^{n}}{\Delta t}-\theta\mathrm{div}\left(\Delta t\nabla p^{n+1,k}\right)=-\mathrm{div}\left(\Theta\left(\rho^{n},\rho^{n+1,k-1}\right)\underline{\tilde{u}}^{k}+\Delta t\left(\underline{\nabla}\,p\big|_{n-1+\theta}^{n+\theta,k-1}\right)\right)+(1-\theta)\mathrm{div}\left(\Delta t\underline{\nabla}\,p\big|_{n-2+\theta}^{n-1+\theta}\right)\\
&\rho^{n+1,k}=\tilde{\rho}^{k}+\left(p^{n+1,k}-p^{n+1,k-1}\right)\left(\frac{\partial\rho}{\partial p}\bigg|_{T}\left(T^{n+1,k},p^{n+1,k-1}\right)\right),\quad \underline{\tilde{u}}^{k}\text{ and }\tilde{\rho}^{k}\text{where are predicted variables.}
\end{aligned}\tag{3}$$

The acoustic waves are treated implicitly, thus removing the acoustic CFL restriction on the time step. An upwind spatial discretization of the equations convective terms lead to a numerical analysis on the positivity of the temperature, pressure and density of a cell c; if the following conditions are below the unity, the positivity is preserved among time for all the aforementioned variables:

$$\begin{aligned}
&CFL_{T_1}^{+}=(1-\theta)\frac{\Delta t}{M_c^n}\sum_{f\in\mathcal{F}_c}\dot{M}_f^{+}\Big|_{n}^{n+1,k-1},\qquad Fo_T^{+}=\frac{\lambda_c(1-\theta)\Delta t}{c_v M_c^n}\sum_{f\in\mathcal{F}_c}|\underline{S}_f|,\\
&CFL_{T_2}^{+}=\frac{\Delta t}{M_c^n}\sum_{f\in\mathcal{F}_c}\left[\theta(\gamma-1)\frac{T_c^{n+1,k-1}}{T_c^n}+(1-\theta)\gamma\right]\dot{M}_f^{+}\Big|_{n}^{n+1,k-1}+\frac{\Delta t(\gamma-1)\underline{u}_c^{n+\theta,k-1}\cdot\underline{\nabla}_c\,p\big|_{n-1+\theta}^{n+\theta,k-1}}{p_c^n},\\
&CFL_{p}^{+}=\frac{\Delta t}{M_c^n}\sum_{f\in\mathcal{F}_c}\left\langle\Theta\left(\rho^{n},\rho^{n+1,k-1}\right)\underline{\tilde{u}}^{k}+\Delta t\underline{\nabla}\,p\big|_{n-1+\theta}^{n+\theta,k-1}\right\rangle_f\cdot\underline{S}_f+(1-\theta)\Delta t\underline{\nabla}_f\,p\big|_{n-2+\theta}^{n-1+\theta}\cdot\underline{S}_f,
\end{aligned}\tag{4}$$

where $\underline{S}_f$ is the outward surface vector, $\dot{M}_f^{+}\Big|_{n}^{n+1}=\max(0,\dot{M}_f\big|_{n}^{n+1})$ the positive contribution of the face mass flux and M_c the cell mass.

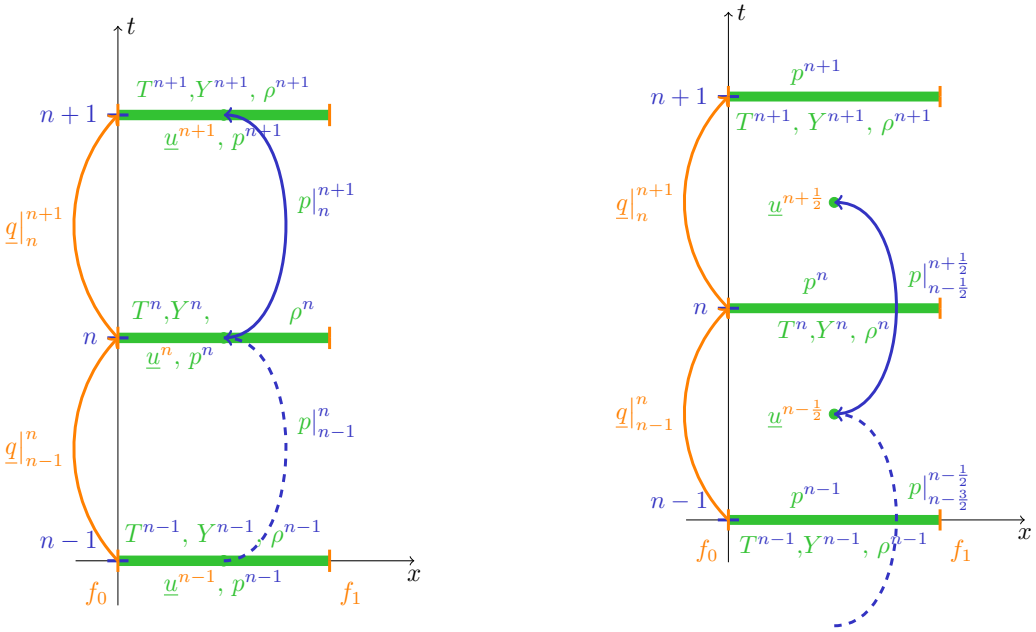

Figure 1: Time discretized variables localisation. Left frame : $\theta=1$. Right frame : $\theta=1/2$.

2 RESULTS

The present scheme is verified and validated along different verification and validation cases. Note that for all test cases, the time step is constant.

2.1 0-D Pressure cooker like cell

A single computational $[1 \times 1 \times 1]\ m^3$ cell with no fluxes is heated by its lateral faces while others are adiabatic. First, the scheme ability to account pressure variations is verified while conserving the mass of the system by imposing a Neumann condition on the walls. Then, its time convergence rate is verified through a Dirichlet condition. The exact temperature expressions for the Neumann (N) and Dirichlet (D) case read:

$$T_{\mathrm{N}}(t) = T_0 \left(1 + \frac{t}{\tau_1}\right), \quad \tau_1 = \frac{\Omega\, \rho_0\, c_v\, T_0}{S\, Q_i}. \qquad T_{\mathrm{D}}(t) = (T_0 - T_w)\ e^{-\frac{t}{\tau_2}} + T_w, \quad \tau_2 = \frac{\Omega\, \rho_0\, c_v}{S\, h}.$$

$T_0 = 300\,\mathrm{K}$ and $\rho_0 = 1.177\,\mathrm{kg\,m^{-3}}$ are the initial temperature and density. Ω is the total cell volume, c_v its heat capacity, and S the total heated wall surface. $T_w = 313\,\mathrm{K}$ denotes the wall temperature and the interior air heat transfer coefficient $h = 30\,\mathrm{W\,m^{-2}\,K^{-1}}$ remains constant. Simulations are performed with a time step $\Delta t = 1\ s$ and one inner iteration. For the Neumann case, the pressure, temperature and density L_2 error norm related to the exact solution are studied over time and compared to a simulation using a Poisson equation to correct the pressure (i.e by considering $\rho^{n+1,k} = \widetilde{\rho}^{k}$ in Eq. (3)). Figure 2, left, shows that the pressure variation is well reproduced by the present scheme and the mass is well conserved. The simulation using the Poisson equation led to more important errors. The increasing behaviour of errors are to be seen as an accumulation of truncation error in the range of the solver precision (10^{-8}). Figure 2, right, shows the pressure L_2 error at $t = 0.8\tau_s$ for the Dirichlet boundary condition study. It is verified that the first and second order time convergence rate are obtained when $\theta = 1$ and $1/2$, respectively.

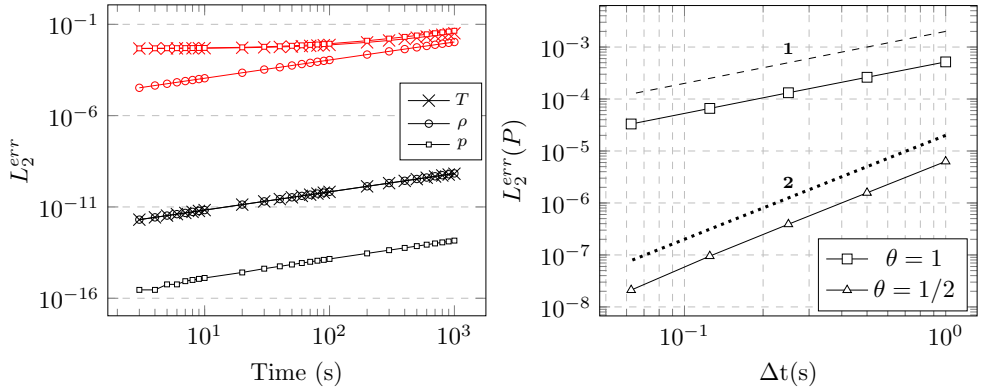

Figure 2: Left: L_2 error norm of the density, temperature and pressure for the Neumann boundary condition case. (–) Poisson scheme. (–) presented scheme. Right: Dirichlet boundary condition case. L2 error for the pressure at $t = 0.8\tau_2$ for a first-order implicit Euler ($\theta = 1$) and Crank Nicolson ($\theta = 1/2$) time scheme.

2.2 Sod shock case

The Sod [11] 1-D Riemann problem is considered to test the scheme accuracy related to singular solutions. Simulations are performed on a tube of length $L = 400\,\mathrm{m}$ with $2^m \times 800$ cells, $0 \leq m \leq 5$. An interface at the middle of the tube is used to initialise the right (R) and left (L) states as following: $\rho_L = 1.0\,\mathrm{kg\,m^{-3}}$, $\rho_R = 0.125\,\mathrm{kg\,m^{-3}}$, $p_L = 100000\,\mathrm{Pa}$ and $p_R = 10000\,\mathrm{Pa}$. Walls are considered as symmetries except the two end faces of the tube, set as outlets. While refining the mesh at two CFL numbers, the variables L_1 error norm at $t = 0.3\,\mathrm{s}$ are studied for both θ values. For each time step, three inner iterations are performed. Figure 3 shows, for a 3200 mesh and $\theta = 1$, the different fields at $t = 0.3\,\mathrm{s}$. The exact solution, in black lines, is accurately reproduced by the simulation using the source term based on the kinetic energy equation (red lines). Even if the density, pressure and velocity fields are close to

the exact solution, the temperature plateau is not achieved without the source term (blue lines). Figure 4 shows for each configuration the variables L_1 error norm related to the exact solution. It is well known that even even second order schemes can not achieve a second order accuracy for irregular solutions. When reducing the cells distance, the time convergence rates tend to 0.5 for the density and temperature and to 1.0 for the pressure and velocity, which are in agreement with these available in the compressible solvers literature [10][12]. Lastly, the presented new CFL like conditions (Eq.4), represented in Figure 5, are shown to be less restraining than the speed based CFL condition.

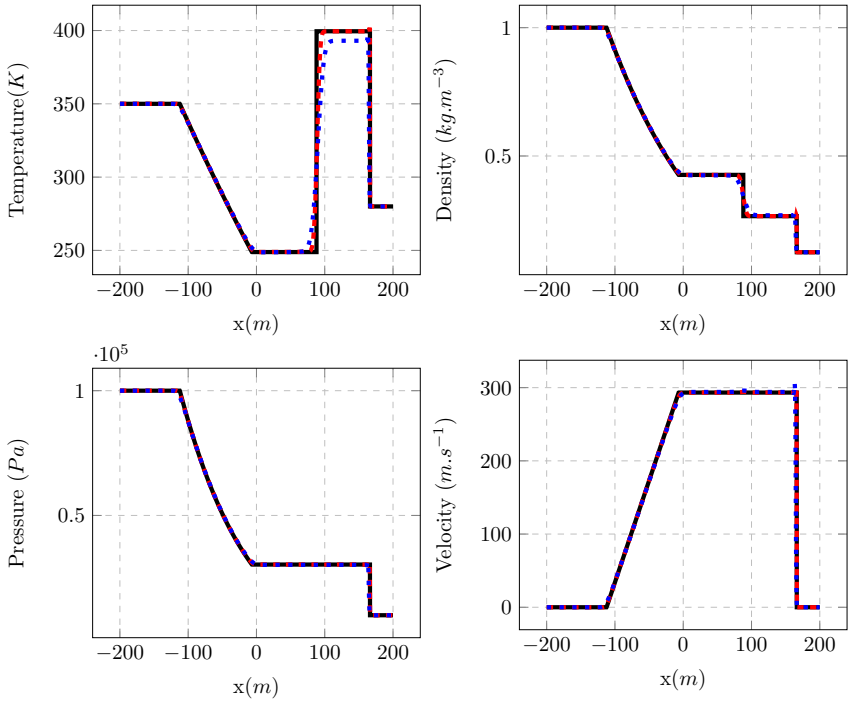

Figure 3: Sod case results at $t = 0.3$ s for $\theta = 1$ using a 3200 cells mesh. (–) exact solution (- -) simulation using the source term $\Gamma^{u^2/2}$ (- -) simulation without the source term $\Gamma^{u^2/2}$.

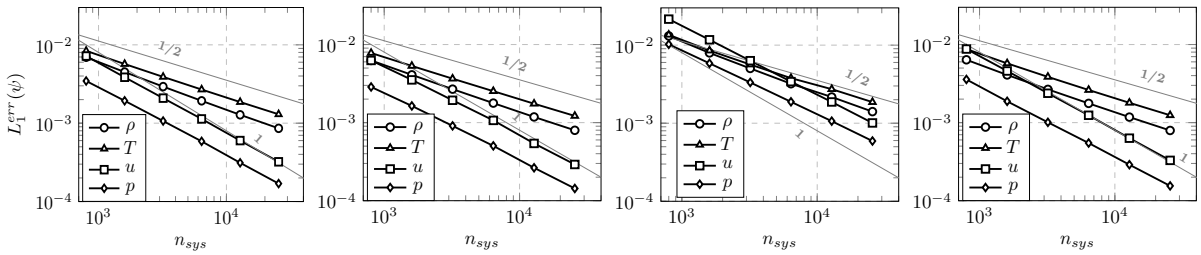

(a) $CFL = 0.04$, $\theta = 1$. (b) $CFL = 0.04$, $\theta = 1/2$. (c) $CFL = 1.0$, $\theta = 1$. (d) $CFL = 1.0$, $\theta = 1/2$.

Figure 4: L_1 error convergence for the SOD case for two values of CFL and θ.

2.3 Natural convection case

A heated cavity numerical benchmark case presented in [13] is studied. The system of characteristic length $L = 0.4603$ m presents a steady flow driven by buoyancy effects at $Ra = 10^6$. The side lateral walls difference of temperature ($T_h = 960$ K and $T_c = 240$ K) is responsible for the cavity motion and the fluid properties are constant. Other walls are considered adiabatic. A 740×740 cells mesh is used

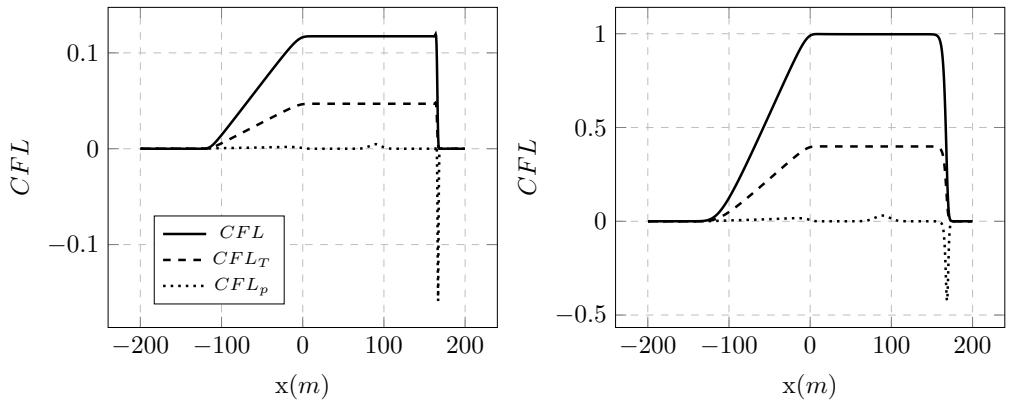

Figure 5: CFL_x numbers for the SOD case for two different velocity based CFL simulations with $\theta = 1$. Left frame: CFL = 0.04. Right frame: CFL = 1.0.

and the mean Nusselt number $\overline{Nu} = \dfrac{1}{L}\displaystyle\int_{y=0}^{y=L} Nu(\mathrm{y})\mathrm{d}y$ evaluated on the cold and hot walls (with $Nu(y) = \dfrac{L}{(T_h - T_c)}\dfrac{\lambda}{\lambda_0}\dfrac{\partial T}{\partial x}\bigg|_w(y)$), and the cavity normalised mean pressure p/p_0 are compared to their reference values. $\lambda_0 = \mu_0\gamma R/((1-\gamma)Pr)$, with $Pr = 0.71$, $\mu_0 = 1.68\times10^{-5}\,\mathrm{kg\,m^{-1}\,s^{-1}}$ and $R = 287\,\mathrm{J\,kg^{-1}\,K^{-1}}$. The time step is fixed to $\Delta t = 0.0025\,\mathrm{s}$ and three inner iterations are performed. To accelerate the convergence to the steady state, the cavity temperature is initialised as $T_0 = 600\,\mathrm{K}$. Figure 6, left, shows that the steady state is reached after 10 s of simulation. Moreover, the normalised density stays constant and equal to the unity, proving the scheme's system mass conservation. The mean pressure reaches as well its reference value of 0.856. Furthermore, the Nusselt number profiles are in agreement to the reference (Figure 6, right), which is reflected by the correct reproduction of the centrelines velocity profiles (Figure 7).

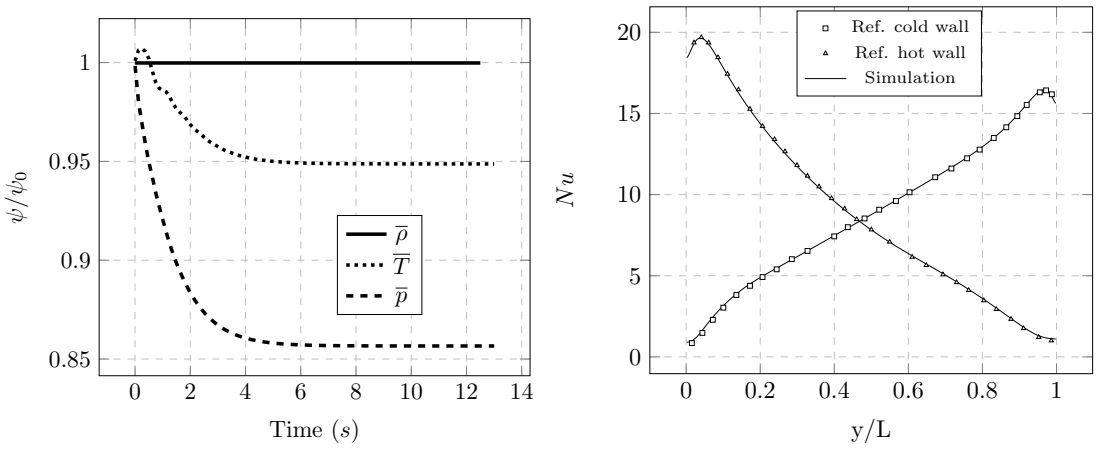

Figure 6: Left: relative domain-averaged quantities ψ/ψ_0 over time. Right: Nusselt number profiles for the hot and cold walls compared to the reference [14].

3 CONCLUSIONS

A staggered time scheme has been proposed, validated and verified against analytical and benchmark problems. A numerical analysis has provided new conditions to insure the positivity of the thermodynamic variables. The latter were shown to be less constraining than the material CFL condition. Further-

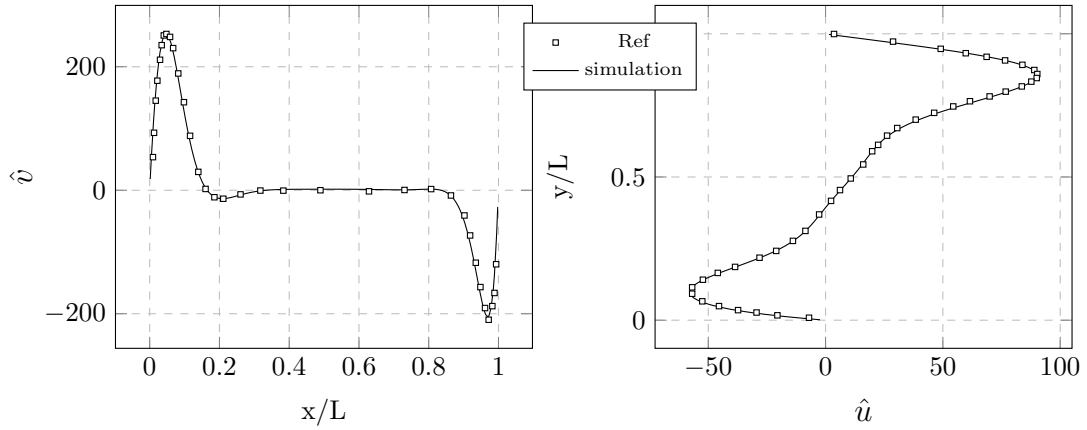

Figure 7: Distribution of the velocity on the centrelines of the convective cavity compared to the reference [14].

more, the presented scheme had good accuracy on accounting pressure variations and reproducing shock and natural convection solutions. An extension of this time scheme to moist-air is in development and further work shall focus on applying the presented scheme to more complex industrial studies.

REFERENCES

[1] H. Guillard & C. Viozat. On the behaviour of upwind schemes in the low Mach number limit. *Computers & fluids*, **28** (1999) 63–86.

[2] P. Degond & M. Tang. All speed scheme for the low Mach number limit of the isentropic Euler equations. *Communications in Computational Physics*, **10** (2011) 1–31.

[3] J. Haack, S. Jin, & J.-G. Liu. An all-speed asymptotic-preserving method for the isentropic Euler and Navier-Stokes equations. *Communications in Computational Physics*, **12** (2012) 955–980.

[4] F. Cordier, P. Degond, & A. Kumbaro. An asymptotic-preserving all-speed scheme for the Euler and Navier–Stokes equations. *Journal of Computational Physics*, **231** (2012) 5685–5704.

[5] W. Boscheri, G. Dimarco, R. Loubère, M. Tavelli, & M.-H. Vignal. A second order all Mach number IMEX finite volume solver for the three dimensional Euler equations. *Journal of Computational Physics*, **415** (2020) 109486.

[6] J. Park & C.-D. Munz. Multiple pressure variables methods for fluid flow at all Mach numbers. *International journal for numerical methods in fluids*, **49** (2005) 905–931.

[7] C. D Pierce & P. Moin. Progress-variable approach for large-eddy simulation of non-premixed turbulent combustion. *Journal of fluid Mechanics*, **504** (2004) 73.

[8] J.-L. Guermond, P. Minev, & J. Shen. An overview of projection methods for incompressible flows. *Computer methods in applied mechanics and engineering*, **195** (2006) 6011–6045.

[9] F. Archambeau, N. Méchitoua, & M. Sakiz. Code Saturne: A finite volume code for the computation of turbulent incompressible flows-Industrial applications. *International Journal on Finite Volumes*, **1**.

[10] R. Herbin, J.-C. Latché, & C. Zaza. A cell-centred pressure-correction scheme for the compressible Euler equations. *IMA Journal of Numerical Analysis*, **40** (2020) 1792–1837.

[11] G. A. Sod. A survey of several finite difference methods for systems of nonlinear hyperbolic conservation laws. *Journal of computational physics*, **27** (1978) 1–31.

[12] C. Colas, M. Ferrand, J.-M. Hérard, J.-C. Latché, & E. Le Coupanec. An implicit integral formulation to model inviscid fluid flows in obstructed media. *Computers & Fluids*, **188** (2019) 136–163.

[13] P. Le Quéré, C. Weisman, H. Paillère, J. Vierendeels, E. Dick, R. Becker, M. Braack, & J. Locke. Modelling of natural convection flows with large temperature differences: a benchmark problem for low Mach number solvers. Part 1. Reference solutions. *ESAIM: Mathematical Modelling and Numerical Analysis*, **39** (2005) 609–616.

[14] M. Darbandi & S.-F. Hosseinizadeh. Numerical simulation of thermobuoyant flow with large temperature variation. *Journal of thermophysics and heat transfer*, **20** (2006) 285–296.